https://doi.org/10.5194/egusphere-2026-2826
Preprint. Discussion started: 11 June 2026

Effects of NO_x on secondary organic aerosol yields and composition from a biogenic–anthropogenic mixture

Guangzhao Xie[1], Aristeidis Voliotis[1,2], Thomas J. Bannan[1], Yunqi Shao[1], Huihui Wu[1*], Dawei Hu[1,2], and Gordon McFiggans[1]

[1]Centre for Atmospheric Science, Department of Earth and Environmental Sciences, School of Natural Sciences, University of Manchester, Manchester, M13 9PL, UK

[2]National Centre for Atmospheric Science (NCAS), University of Manchester, Manchester, M13 9PL, UK

*Now at: Univ Paris Est Créteil and Université Paris Cité, CNRS, LISA, 94010 Créteil, France

Correspondence to: Gordon McFiggans (g.mcfiggans@manchester.ac.uk) and Aristeidis Voliotis (aristeidis.voliotis@manchester.ac.uk)

https://doi.org/10.5194/egusphere-2026-2826
Preprint. Discussion started: 11 June 2026

Abstract

Nitrogen oxides (NO_x = NO_2 + NO) play a crucial role in secondary organic aerosol (SOA) formation. The effects of NO_x on SOA formation from single precursors have been extensively studied. However, in the real atmosphere, biogenic and anthropogenic precursors often coexist, and it remains unclear whether the effects of NO_x in such mixtures can be directly extrapolated from those observed in single-precursor systems. In this study, we investigated the effects of NO_x on SOA particle mass yields and chemical composition from α-pinene, n-dodecane, and their mixture under high- and moderate-NO_x conditions in the Manchester Aerosol Chamber. The results show that SOA particle mass yields were higher under high-NO_x conditions across all systems. Enhanced oxidant levels and alkoxy radical (RO) isomerisation appear to more than compensate for the negative impacts associated with the formation of more volatile products via the reaction of organic peroxy radicals (RO_2) with NO. However, compared with the single-precursor systems, the increase in SOA particle mass yields in the mixed-precursor system was less pronounced. In the mixed-precursor system, enhancement of RO_2 + NO termination pathways was stronger, and the contribution of α-pinene-derived alkoxy-peroxy pathway may have been comparatively weaker. These changes would be expected to favour the formation of more volatile products and thus suppress SOA formation. Collectively, these observations provide evidence that the effects of NO_x in the mixed-precursor systems cannot be interpreted as a simple combination of behaviours observed in individual precursor systems.

https://doi.org/10.5194/egusphere-2026-2826
Preprint. Discussion started: 11 June 2026

1 Introduction

Atmospheric secondary organic aerosol (SOA) is a significant component of fine particulate matter and plays an important role in air quality, climate, and human health (Hallquist et al., 2009; Jimenez et al., 2009; Ramanathan et al., 2001). The precursors of SOA include gas-phase organic compounds emitted from both biogenic and anthropogenic sources (Kanakidou et al., 2005; Srivastava et al., 2022). These compounds undergo oxidation to form less volatile products, which can subsequently partition into the particle phase, leading to the formation of SOA particles (Atkinson and Arey, 2003; Baltensperger et al., 2005; Kroll and Seinfeld, 2008; Robinson et al., 2007). In the atmosphere, these processes can be influenced by the presence of inorganic trace gases and other SOA precursors (Atkinson, 2003; McFiggans et al., 2019; Ziemann and Atkinson, 2012). Such complexity makes it challenging to achieve a comprehensive understanding and accurate prediction of SOA formation.

Nitrogen oxides (NO_x = NO_2 + NO) are important trace gases in the atmosphere and play a critical role in SOA formation (Atkinson, 2000; Lane et al., 2008; Ziemann and Atkinson, 2012). On the one hand, NO can react with peroxy radicals (RO_2), forming organic nitrates ($RONO_2$) and alkoxy radicals (RO) (Ziemann and Atkinson, 2012). RO radicals can subsequently undergo fragmentation, isomerisation, or reaction with O_2 (Orlando et al., 2003). NO_2 can react with RO_2 to form peroxynitrates (RO_2NO_2). On the other hand, NO_x modulates O_3 and OH levels through its interactions with RO_x radicals (RO_x = OH + HO_2 + RO_2) (Atkinson, 2003; Chen et al., 2022; Clapp and Jenkin, 2001; Pusede et al., 2015). O_3 concentrations depend strongly on the relative abundance of SOA precursors to NO_x (Chen et al., 2022). Since O_3 photolysis is an important source of OH radicals, NO_x can indirectly influence OH formation by controlling O_3 levels (Pullinen et al., 2020). In addition, NO_x can alter OH concentrations through the reactions HO_2 + NO → OH + NO_2 and OH + NO_2 → HNO_3 (Chen et al., 2022). These factors collectively influence SOA formation and may either enhance or suppress SOA particle mass yields.

α-Pinene ($C_{10}H_{16}$), which constitutes nearly 50% of global monoterpene emissions, is considered one of the most important biogenic SOA precursors in the troposphere (Andreae and Crutzen, 1997; Lee et al., 2006; Pathak et al., 2007). The effects of NO_x on SOA formation from α-pinene have been extensively investigated (Eddingsaas et al., 2012; Ng et al., 2007; Stirnweis et al., 2017; Zhao et al., 2018). It is generally recognised that NO_x can suppress SOA formation from α-pinene. This suppression is typically attributed to the formation of more volatile products formed via RO_2 + NO reactions compared with those formed through RO_2 + HO_2 or RO_2 + RO_2 pathways. Increasing attention has recently been directed towards the effects of NO_x on highly oxygenated molecules (HOMs), which are formed through the autoxidation of RO_2 radicals and are considered important contributors to SOA formation (Bianchi et al., 2019; Ehn et al., 2014; Kang et al., 2025; Pospisilova et al., 2020; Pullinen et al., 2020). Pullinen et al. (2020) showed that NO_x suppresses the formation of HOM accretion products and thus reduces SOA formation potential. More recently, several studies have reported that NO may also enhance HOM formation by promoting RO radical formation, allowing continued autoxidation through RO isomerisation (Kang et al., 2025; Nie et al.,

https://doi.org/10.5194/egusphere-2026-2826
Preprint. Discussion started: 11 June 2026

2023). This enhancement may partially compensate for the RO_2 sink introduced by NO. Although first-generation RO radicals derived from α-pinene predominantly undergo C–C bond scission, isomerisation of HOM-RO radicals can compete with fragmentation, thereby contributing to radical chain propagation (Dibble, 2001; Kang et al., 2025; Vereecken and Peeters, 2010).

When the influence of NO_x on oxidant concentrations is also considered, the effects become more complex. Modelling studies have shown that biogenic SOA formation can be enhanced under increasing NO_x levels on a regional scale, due to the increases in OH and O_3 concentrations (Pye et al., 2019). Laboratory studies have also demonstrated the important role of NO_x in modulating oxidant levels. Sarrafzadeh et al. (2016) observed an increase in SOA yields with rising NO_x concentrations under low-NO_x conditions, which was attributed to enhanced OH concentrations. Therefore, the effect of NO_x on SOA formation arises from its combined influence on oxidant levels and RO_2 radical chemistry. Both factors should be considered when investigating NO_x-related processes.

SOA formed from anthropogenic precursors makes a significant contribution to the total SOA burden in urban environments (Kelly et al., 2018). Alkanes constitute an important fraction of anthropogenic gas-phase organic compounds. Previous studies have shown that, for some long-chain alkanes, SOA particle mass yields increase with increasing NO_x concentrations under comparable OH exposures (Loza et al., 2014). This behaviour was attributed to the preference of RO radicals for isomerisation over fragmentation, thereby preserving the carbon backbone and promoting the formation of lower-volatility products (Lim and Ziemann, 2009). Recent studies have further suggested that HOM yields from alkane oxidation increase with NO concentrations, likely reflecting the enhanced importance of RO radical isomerisation (Wang et al., 2021).

However, these findings are derived from single-precursor systems. In the real atmosphere, NO_x is often co-emitted with other anthropogenic SOA precursors. Existing studies have shown that the coexistence of multiple precursors can also simultaneously influence oxidant levels and RO_2 radical reaction pathways, ultimately influencing SOA particle mass yields. For example, McFiggans et al. (2019) demonstrated that mixing α-pinene with isoprene substantially suppresses SOA formation from α-pinene. This suppression was attributed to competition for available OH by isoprene and the scavenging of α-pinene-derived HOM-RO_2 radicals. More recent studies have investigated systems involving both biogenic and anthropogenic precursors and reported that the overall SOA particle mass yields in these mixtures deviate from values predicted by additive calculations (Voliotis et al., 2022). These observations suggest that non-linear effects may arise when multiple precursors coexist. Therefore, in mixed-precursor systems, the effects of NO_x on SOA formation may not be directly extrapolated from those observed in single-precursor systems. To accurately predict SOA formation, it is necessary to consider not only the effects of NO_x but also the interactions between different precursors. However, studies investigating the effects of NO_x on SOA formation in mixed-precursor systems remain limited.

https://doi.org/10.5194/egusphere-2026-2826
Preprint. Discussion started: 11 June 2026

In this study, we investigated the effects of NO_x on SOA particle mass yields and chemical composition from α-pinene, n-dodecane, and their mixture in the Manchester Aerosol Chamber (MAC). n-Dodecane ($C_{12}H_{26}$) is a representative long-chain alkane primarily emitted from diesel fuel combustion (Zhao et al., 2015). High-resolution mass spectrometry was used to directly characterise the product distribution at the level of chemical formula in the particle phase. Based on changes in the fractions of CHON and fragmented products, as well as shifts in the oxygen-number parity of representative products, we inferred the influence of NO_x on radical chemistry. Combined with the effects of NO_x on oxidant levels, these observations further suggested potential implications for SOA particle mass yields.

https://doi.org/10.5194/egusphere-2026-2826
Preprint. Discussion started: 11 June 2026

Table 1. Summary of experimental conditions.

Experiment No.	Experiment Type	$[n\text{-dodecane}]_0$[a] (ppb)	$[\alpha\text{-pinene}]_0$[a] (ppb)	$[NO_x]_0$[a] (ppb)	$[precursor]_0$[a] $/[NO_x]_0$	$[Seed]_0$[a] ($\mu g\ m^{-3}$)	$[O_3]_{max}$ (ppb)	SOA ($\mu g\ m^{-3}$)	SOA particle mass yields
			α-Pinene experiments						
1	α-pinene (high NO_x)	-	59.4	57	1.0	31.0	37.9	39.9	0.12
2	α-pinene (high NO_x)	-	48.9	54	0.9	56.1	39.0	42.1	0.16
3	α-pinene (moderate NO_x)	-	41.6	17	2.4	44.6	10.1	11.0	0.08
4	α-pinene (moderate NO_x)	-	41.9	21	2.0	45.8	15.4	13.1	0.06
			n-dodecane experiments						
5	n-dodecane (high NO_x)	160	-	281	0.6	37.8	103.1	177.5	NA[b]
6	n-dodecane (high NO_x)	160	-	156	1.0	31.2	98.4	122.9	0.17
7	n-dodecane (moderate NO_x)	160	-	63	2.5	29.2	61.1	49.0	0.09
8	n-dodecane (moderate NO_x)	160	-	55	2.9	16.3	53.4	34.3	NA[b]
			Mixed-precursor experiments						
9	Mixture (high NO_x)	80	24.8	160	0.7	34.5	85.9	71.4	NA[b]
10	Mixture (high NO_x)	80	27.4	121	0.9	36.9	76.2	63.9	0.11
11	Mixture (moderate NO_x)	80	13.4	47	2.0	34.2	42.2	29.4	0.08

[a] The subscript "0" indicates the initial concentration.

[b] NA: no available data.

https://doi.org/10.5194/egusphere-2026-2826
Preprint. Discussion started: 11 June 2026

2 Methodology

2.1 Diagnostic tools for peroxy radical chemistry

RO_2 radicals are key intermediate species in atmospheric chemistry. Relevant reaction pathways have been extensively described in previous studies (Atkinson, 2000; Ziemann and Atkinson, 2012).

In the absence of NO_x, RO_2 mainly react with HO_2 or with other RO_2 radicals, forming closed-shell products such as hydroperoxides, carbonyls, alcohols, and accretion products (Atkinson, 2000; Ziemann and Atkinson, 2012). The presence of NO_x introduces additional reaction pathways leading to the formation of organic nitrates and peroxynitrates (Atkinson, 2000). Consequently, increasing NO_x concentrations are expected to enhance the contribution of CHON compounds. However, as peroxynitrates are generally thermally unstable at room temperature, this study primarily focuses on the RO_2 + NO pathway.

In addition to forming closed-shell products, reactions of RO_2 with RO_2, NO, and potentially HO_2 can also generate RO radicals (Orlando et al., 2003). Among these pathways, reaction with NO proceeds rapidly and strongly favours RO formation, making RO_2 + NO an important source of RO radicals in the presence of NO_x. The resulting RO radicals can subsequently undergo fragmentation, isomerisation or reaction with O_2. However, for α-pinene and n-dodecane systems, the RO + O_2 pathway is generally considered to be of minor importance and is therefore not discussed further here (Ziemann and Atkinson, 2012).

For primary RO radicals derived from α-pinene, the relatively low energy barrier for C-C bond scission favours fragmentation (Dibble, 2001). Accordingly, products with carbon numbers lower than 10 in the α-pinene system are used here as indicators of RO chemistry. In principle, increasing NO_x concentrations are expected to enhance the relative importance of the RO_2 + NO pathway, thereby promoting RO chemistry and increasing the fraction of fragmentation products.

For some long-chain and highly functionalised RO radicals, isomerisation can also represent an important reaction pathway (Lim and Ziemann, 2009; Ziemann and Atkinson, 2012). Following formation from RO_2, RO radicals can undergo isomerisation and subsequent O_2 addition, regenerating RO_2 radicals. This process, commonly referred to as the alkoxy-peroxy pathway, alters the oxygen-number parity of the resulting RO_2 radicals (Kang et al., 2025). Such shifts in oxygen-number parity can therefore serve as indicators of the extent of RO isomerisation. As RO_2 radicals were not directly measured in this study, the oxygen-number parity of representative closed-shell products is used as a diagnostic proxy.

For α-pinene, $C_{10}H_{15}O_x$ and $C_{10}H_{17}O_x$ are expected to be the major RO_2 families (Berndt et al., 2016; Jenkin et al., 1997; Johnson and Marston, 2008; Kang et al., 2025; Vereecken and Peeters, 2004). Within the $C_{10}H_{17}O_x$ family, the first-generation RO_2 radical is $C_{10}H_{17}O_3$. Through autoxidation, this radical evolves into a series of $C_{10}H_{17}O_x$ RO_2 radicals containing odd

https://doi.org/10.5194/egusphere-2026-2826
Preprint. Discussion started: 11 June 2026

numbers of oxygen atoms (hereafter denoted as $C_{10}H_{17}O_{2x+1}$). When these RO_2 radicals react with NO, they form $C_{10}H_{17}NO_{2x}$ products with even numbers of oxygen atoms. If any of $C_{10}H_{17}O_{2x+1}$ RO_2 radicals undergo an alkoxy-peroxy pathway, their oxygen-number parity shifts from odd to even, forming $C_{10}H_{17}O_{2x}$ RO_2. Subsequent reaction of these radicals with NO produces $C_{10}H_{17}NO_{2x+1}$ products with odd numbers of oxygen atoms. For $C_{10}H_{15}O_x$ family, the autoxidation chain is assumed to begin with $C_{10}H_{15}O_4$, generating a series of $C_{10}H_{15}O_x$ RO_2 radicals with even numbers of oxygen atoms (hereafter denoted as $C_{10}H_{15}O_{2x}$). Reaction of these radicals with NO forms $C_{10}H_{15}NO_{2x+1}$ products with odd numbers of oxygen atoms. If these RO_2 radicals undergo an alkoxy-peroxy pathway, their oxygen-number parity shifts from even to odd, forming $C_{10}H_{15}O_{2x+1}$ RO_2 radicals. Termination of these radicals with NO yields $C_{10}H_{15}NO_{2x}$ products with even numbers of oxygen atoms. Therefore, the oxygen-number parity of $C_{10}H_{17}NO_n$ and $C_{10}H_{15}NO_n$ can be used to diagnose the importance of RO isomerisation in the α-pinene system. An enhancement in RO isomerisation is expected to increase the fraction of $C_{10}H_{17}NO_n$ products with odd numbers of oxygen atoms and $C_{10}H_{15}NO_n$ products with even numbers of oxygen atoms within their respective product families.

For n-dodecane, $C_{12}H_{25}O_x$ are expected to be the major RO_2 family (Zhang et al., 2014). Within this family, the first-generation RO_2 radical is $C_{12}H_{25}O_2$. Through autoxidation, this radical evolves into a series of $C_{12}H_{25}O_x$ RO_2 radicals containing even numbers of oxygen atoms (hereafter denoted as $C_{12}H_{25}O_{2x}$). When these RO_2 radicals react with NO, they form $C_{12}H_{25}NO_{2x+1}$ products with odd numbers of oxygen atoms. If any of these RO_2 radicals undergo the alkoxy-peroxy pathway, their oxygen-number parity shifts from even to odd, forming $C_{12}H_{25}O_{2x+1}$ RO_2 radicals. Subsequent reaction of these radicals with NO produces $C_{12}H_{25}NO_{2x}$ products with even numbers of oxygen atoms. Therefore, the oxygen-number parity of $C_{12}H_{25}NO_n$ products can be used to diagnose the importance of RO isomerisation in the n-dodecane system. An enhancement in RO isomerisation is expected to increase the fraction of $C_{12}H_{25}NO_n$ products with even numbers of oxygen atoms within this product family.

However, if an even number of alkoxy-peroxy steps occurs, the original oxygen-number parity is restored, making these products indistinguishable from those formed without undergoing this pathway. Consequently, this approach cannot distinguish between RO_2 radicals that have undergone an even number of alkoxy-peroxy steps and those that have not undergone this process. Despite this limitation, the approach can still provide meaningful insight when multiple alkoxy-peroxy steps are not prevalent.

2.2 Manchester Aerosol Chamber

The experiments were conducted in the MAC at the University of Manchester. A detailed description of the chamber is provided in Shao et al. (2022). The MAC is an 18 m^3 fluorinated ethylene propylene (FEP) Teflon chamber operated in batch mode, providing a closed system without continuous inflow of reactants or clean air. The Teflon bag is supported by aluminium

https://doi.org/10.5194/egusphere-2026-2826
Preprint. Discussion started: 11 June 2026

frames, with the upper and lower frames being movable, allowing the chamber volume to expand or collapse. This design maintains constant pressure inside the chamber and prevents sampling-induced dilution.

All the reactants (SOA precursors, NO_x, and seed) were injected into the chamber and mixed thoroughly before the start of the photochemical experiment. The desired amount of liquid SOA precursors (α-pinene, analytical standard, Sigma-Aldrich; n-dodecane, anhydrous, ≥ 99.0 %, Sigma-Aldrich) were introduced into a heated glass bulb using a syringe to facilitate vaporisation and were subsequently carried into the chamber by N_2. NO_x was introduced from a custom-made cylinder, using N_2 as the carrier gas. Seed aerosols were generated by nebulising aqueous ammonium sulfate solutions ($(NH_4)_2SO_4$, ACS reagent, ≥ 99.0 %, Sigma-Aldrich) with an atomiser (ATM 230, Topas), passed through an aerosol residence chamber, and then introduced into the chamber.

The chamber was illuminated by two fixed light sources comprising two xenon arc lamps (XBO 6000W/HSLA OFR, Osram) and a series of halogen lamps (50W/4700K MR16, Solux), which provide irradiation over the wavelength range of 290–800 nm to approximate the atmospheric radiation spectrum. In addition, to enhance OH radical production, a UVC lamp (TUV 130W XPT SE UNP/20, Philips) was installed, with over 90 % of its length covered to minimise its contribution to the overall irradiation.

2.3 Experimental conditions and procedures

Table 1 summarises the key experimental conditions and results. All experiments were conducted at a relative humidity of 50 ± 5 % and a temperature of approximately 25 °C in the presence of $(NH_4)_2SO_4$ seed particles (36.1 ± 10.3 μg m^{-3}). Experiments were performed under two NO_x conditions (Fig. S1). For the high-NO_x experiments, the initial precursor/NO_x ratios ranged from 0.6 to 1.0, while for the moderate-NO_x experiments, the ratios ranged from 2.0 to 2.9.

NO_2 served as the source of O_3, and the subsequent O_3 photolysis in the moist chamber atmosphere generated OH radicals, thereby initiating the photochemical oxidation. OH radicals were the primary oxidant in our experiments. On average, OH oxidation accounted for approximately 80% of α-pinene decay, while ozonolysis contributed the remaining 20%. In contrast, n-dodecane lacks double bonds and therefore reacts only with OH. The estimated OH concentrations (2–6 × 10^6 molecules cm^{-3}) were within the range typically observed in the atmosphere (Fig. S2). Details of the estimation method are provided in Xie et al. (2025).

To control the photochemical conditions across different systems, all experiments were designed to have comparable initial reactivity towards OH radicals, referred to as iso-reactivity. In the mixed-precursor system, α-pinene and n-dodecane were also configured to achieve iso-reactivity. This reactivity depends on precursor concentrations and their reaction rate constants with

https://doi.org/10.5194/egusphere-2026-2826
Preprint. Discussion started: 11 June 2026

OH. The concept of iso-reactivity has been described in detail in previous studies (Voliotis et al., 2022; Voliotis et al., 2021). The rate coefficients for α-pinene and n-dodecane with OH are 5.33×10^{-11} and 1.32×10^{-11} cm^3 $molecule^{-1}$ s^{-1}, respectively (Atkinson, 2003; Dash et al., 2014). Consequently, larger initial concentrations of n-dodecane were required to achieve iso-reactivity. The target mixing ratios of α-pinene were set to 40 ppb in the single-precursor experiments and 20 ppb in the mixed-precursor system, whereas those of n-dodecane were set to 160 and 80 ppb, respectively. Under idealised iso-reactivity conditions, each precursor molecule would initially have an equal probability of reacting with OH. However, as the reactions progressed, the presence of O_3, together with the differing reaction rates of individual precursors towards O_3, caused precursor decay and, consequently, OH reactivity to diverge. For systems involving multiple precursors and oxidants, maintaining fully comparable reaction conditions is inherently challenging. Nevertheless, these evolving chemical regimes, to some extent, reflect the complexity of conditions in the real atmosphere.

Each photochemical experiment followed a four-stage procedure: (i) pre-experiment, during which the chamber underwent repeated flush-fill cycles for approximately 1.5 h to minimise background concentrations before all reactants were introduced; (ii) stabilisation, during which the chamber was kept in the dark for 20–30 min to allow the initial conditions to stabilise; (iii) experiment, during which photochemical reactions proceeded for approximately 5 h; and (iv) post-experiment, during which the lights were turned off and the chamber underwent repeated flush-fill cycles for approximately 1 h, followed by filling the chamber with O_3 (≥1 ppm) and leaving it overnight to oxidise residual O_3-reactive species.

2.4 Instrumentation

Gas- and particle-phase chemical compositions were measured using a Filter Inlet for Gases and Aerosols coupled to a Chemical Ionisation Time-of-Flight Mass Spectrometer (FIGAERO-CIMS, Aerodyne Research Inc.) (Bannan et al., 2019; Lopez-Hilfiker et al., 2014). The instrument was operated in negative-ion mode using iodide (I^-) as the reagent ion. Measurement were conducted in cyclic mode with a cycle duration of 1.5 h, following the sequence: (i) gas-phase sampling with simultaneous particle collection (30 min); (ii) temperature-programmed thermal desorption of collected particles (25 min); (iii) isothermal soaking (15 min); (iv) cooling (20 min); and (v) cleaning (2 min). Each experiment consisted of four such cycles, and the results presented in this study correspond to the final cycle of each experiment. Data were processed using the Tofware package (v4.0.0) within Igor Pro 7.0.8 (WaveMetrics©). Peak fitting was performed for iodide adducts within the m/z range of 200–550, which account for most of the total signal. Chamber and instrument background measurement were performed to correct for potential interferences. Further details of the background measurements are provided in Xie et al. (2025).

Gaseous SOA precursors were measured using a Vocus Proton-Transfer-Reaction Time-of-Flight Mass Spectrometer (Vocus PTR-ToF-MS, Tofwerk) (Krechmer et al., 2018; Yuan et al., 2017). The ion source was supplied with a 20 sccm flow of water

https://doi.org/10.5194/egusphere-2026-2826
Preprint. Discussion started: 11 June 2026

vapour. The ion-molecule reactor (IMR) was maintained at 60 °C and 2.0 mbar, with an axial voltage of 568 V and an RF amplitude of 450 V at 1.3 MHz, corresponding to a reduced electric field strength (E/N) of 141 Td. Data acquisition was carried out in repeating 5 min cycles consisting of 4 min of sampling and 1 min of instrumental background measurement. The α-pinene concentration was calibrated prior to each experiment. Due to the absence of an n-dodecane gas standard, its initial mixing ratios were assumed to correspond the target values (160 ppb in the single-precursor system and 80 ppb in the mixed-precursor system). The consumption of n-dodecane was tracked using the fragment ion $C_{10}H_{21}^+$ as a representative tracer. However, contributions to this ion signal from other oxidation products or fragment ions cannot be fully excluded, which may have resulted in an underestimation of n-dodecane consumption (Xie et al., 2025). Nevertheless, the overall trends in SOA particle mass yields are unlikely to be significantly affected by this uncertainty.

Non-refractory aerosol particles were measured using a Compact Time-of-Flight Aerosol Mass Spectrometer (C-ToF-AMS, Aerodyne Research Inc.) (Drewnick et al., 2009). Ionisation efficiency (IE) and relative ionisation efficiency (RIE) calibrations were conducted using size-selected NH_4NO_3 and $(NH_4)_2SO_4$ particles. The average IE value for NH_4NO_3 was 2.75×10^{-7} ions molecule^{-1}, and the RIE values for NH_4^+ and SO_4^{2-} were 4.71 ± 0.24 and 1.13 ± 0.01, respectively. SOA particle wall losses were corrected using the OA/sulfate correction method (Wang et al., 2018).

NO and NO_2 were measured using a chemiluminescence NO-NO_2-NO_x analyser (Model 42i, Thermo Fisher Scientific Inc.). O_3 was monitored using a UV absorption O_3 analyser (Model 49C, Thermo Fisher Scientific Inc.). Seed aerosol mass concentrations in the 20–500 nm size range was determined using a Differential Mobility Particle Sizer (DMPS) consisting of a Vienna-design differential mobility analyser (DMA) coupled to a Condensation Particle Counter (CPC, model 3775, TSI Inc.).

https://doi.org/10.5194/egusphere-2026-2826
Preprint. Discussion started: 11 June 2026

3 Results

3.1 Formation of O_3 and SOA particles

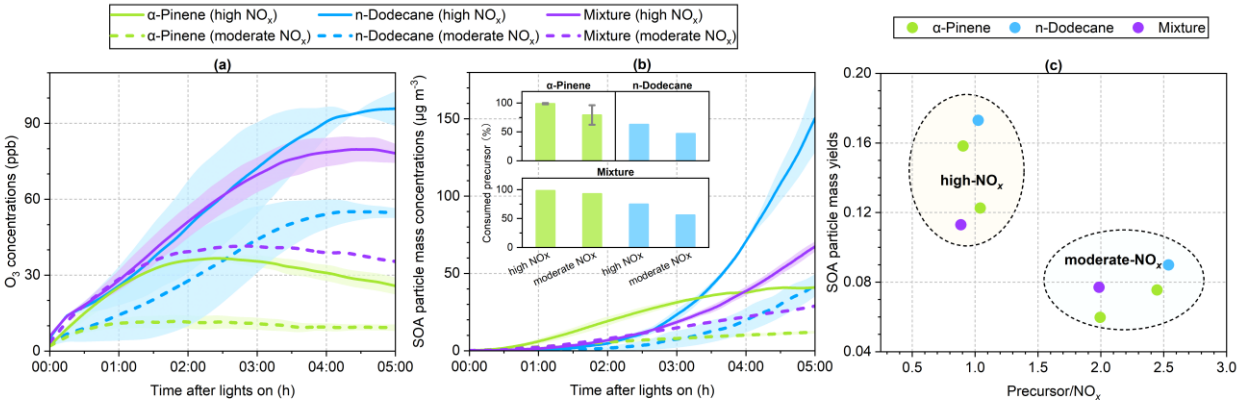

Figure 1: Time series of (a) O_3 concentrations and (b) SOA particle mass concentrations during the photooxidation of α-pinene, n-dodecane, and their mixture under different NO_x conditions. Solid and dashed lines denote experiments conducted under high- and moderate-NOx conditions, respectively. Where duplicate experiments were available, the lines represent the mean values, and the shaded area indicates the range between replicates. The insets in panel (b) show the percentage of precursor consumed at the end of each experiment. The error bars represent ±1 standard deviation derived from duplicate α-pinene experiments, for which replicate PTR-MS measurements were available. Panel (c) summarises SOA particle mass yields as a function of the initial precursor/NO_x ratios.

Figure 1a and 1b present the time series of O_3 and SOA particle mass concentrations for the α-pinene, n-dodecane, and mixture systems under different NO_x conditions. Overall, systems with lower precursor/NO_x ratios exhibited higher O_3 concentrations and SOA particle mass yields (Fig. 1c).

In the α-pinene system, the average α-pinene/NO_x ratio under high-NO_x conditions was 1.0. Upon initiation of photochemical reactions, O_3 concentration increased rapidly, reaching a peak of 38.5 ppb within 2.5 h, after which it gradually decreased. By the end of the experiment, nearly all α-pinene had been consumed, forming approximately 41.0 μg m^{-3} of SOA particles, corresponding to an average mass yield of 0.14. Under moderate-NO_x conditions (α-pinene/NO_x ≈ 2.2), O_3 reached a lower peak of 12.7 ppb after approximately 1 h and remained relatively stable thereafter. By the end of the experiment, on average 21 % of α-pinene remained unreacted, and SOA particle mass reached 12.1 μg m^{-3}, corresponding to a mass yield of 0.07.

For the n-dodecane system, the n-dodecane/NO_x ratios were approximately 0.8 under high-NO_x conditions and 2.7 under moderate-NO_x conditions. O_3 concentrations were substantially higher than those in the α-pinene experiments, reaching 96.3

https://doi.org/10.5194/egusphere-2026-2826
Preprint. Discussion started: 11 June 2026

and 55.7 ppb after approximately 4 h under high- and moderate-NO_x conditions, respectively. Under high-NO_x conditions, 37 % of n-dodecane remained unreacted at the end of the experiment, producing 122.9 μg m^{-3} of SOA particles, corresponding to a mass yield of 0.17 (Exp. 5). Under moderate-NO_x conditions, 53 % of n-dodecane remained unreacted, and SOA particle mass reached 49.0 μg m^{-3}, corresponding to a mass yield of 0.09 (Exp. 7).

In the mixture, the precursor/NO_x ratios were approximately 0.8 under high-NO_x conditions and 2.0 under moderate-NO_x conditions. Peak O_3 concentrations were intermediate between those observed in the single-precursor systems. Under high-NO_x conditions, O_3 peaked at 81.1 ppb after about 4 h of reaction. By the end of the experiment, α-pinene was almost completely consumed, whereas 25 % of n-dodecane remained unreacted, and SOA particle mass reached 63.9 μg m^{-3}, corresponding to a mass yield of 0.11 (Exp. 10). Under moderate-NO_x conditions, O_3 reached a maximum of 42.2 ppb after approximately 2.5 h. By the end of the experiment, 44 % of n-dodecane and 7 % of α-pinene remained unreacted, and SOA particle mass reached 29.4 μg m^{-3}, corresponding to a mass yield of 0.08.

3.2 Chemical composition of SOA particles

3.2.1 α-Pinene

Figure 2 presents the high-resolution mass spectra of particle-phase products measured by FIGAERO-CIMS in α-pinene experiments under high- and moderate-NO_x conditions, together with the corresponding difference spectra. The detected products were mainly distributed within the molecular mass range of 150–280 Da.

CHO compounds dominated the particle-phase composition. Under moderate-NO_x conditions, CHON compounds accounted for only 7 % of the total signal, whereas their contribution increased to 12 % under high-NO_x conditions.

α-Pinene-derived products with fewer than 10 carbon atoms were classified as fragments, those with 10 carbon atoms as monomers, and those with more than 10 carbon atoms as accretion products. Under moderate-NO_x conditions, these three groups contributed 55 %, 30 %, and 15 %, respectively, whereas under high-NO_x conditions their proportions shifted to 63 %, 25 %, and 12 % (Fig. 2). Fragments were the dominant group. Among these, C_7 - C_9 CHO compounds made the largest contribution (Fig. S3), including species such as $C_9H_{12,14}O_6$, $C_8H_{12}O_{4\text{-}6}$, and $C_7H_{10}O_{4\text{-}5}$. Monomers were primarily composed of CHO compounds such as $C_{10}H_{14}O_{4\text{-}7}$ and $C_{10}H_{16}O_{6\text{-}7}$, along with several CHON compounds (e.g. $C_{10}H_{15}NO_{7\text{-}8}$). Accretion products such as $C_{19}H_{28}O_{7\text{-}8}$ were detected; however, their overall contribution was relatively low.

NO_x conditions significantly influenced the distribution of CHON and CHO compounds across carbon-number groups (Fig. 3a). Under high-NO_x conditions, fragment-CHO (frag-CHO) and fragment-CHON (frag-CHON) compounds increased by 5.8 and 3.1 percentage points, respectively. The fraction of monomer-CHO (mon-CHO) compounds decreased by 7.4 percentage

https://doi.org/10.5194/egusphere-2026-2826
Preprint. Discussion started: 11 June 2026

points, whereas monomer-CHON (mon-CHON) compounds increased by 2.0 percentage points. The contribution of accretion-CHO (acc-CHO) compounds also decreased by 3.5 percentage points.

Figure 4a shows the oxygen-number parity of $C_{10}H_{17}NO_n$ and $C_{10}H_{15}NO_n$ under different NO_x conditions. The fraction of $C_{10}H_{17}NO_n$ with an odd number of oxygen atoms increased markedly from 40 % under moderate-NO_x conditions to 70 % under high-NO_x conditions. The fraction of $C_{10}H_{15}NO_n$ with an even number of oxygen atoms increased slightly from 59 % to 61 %.

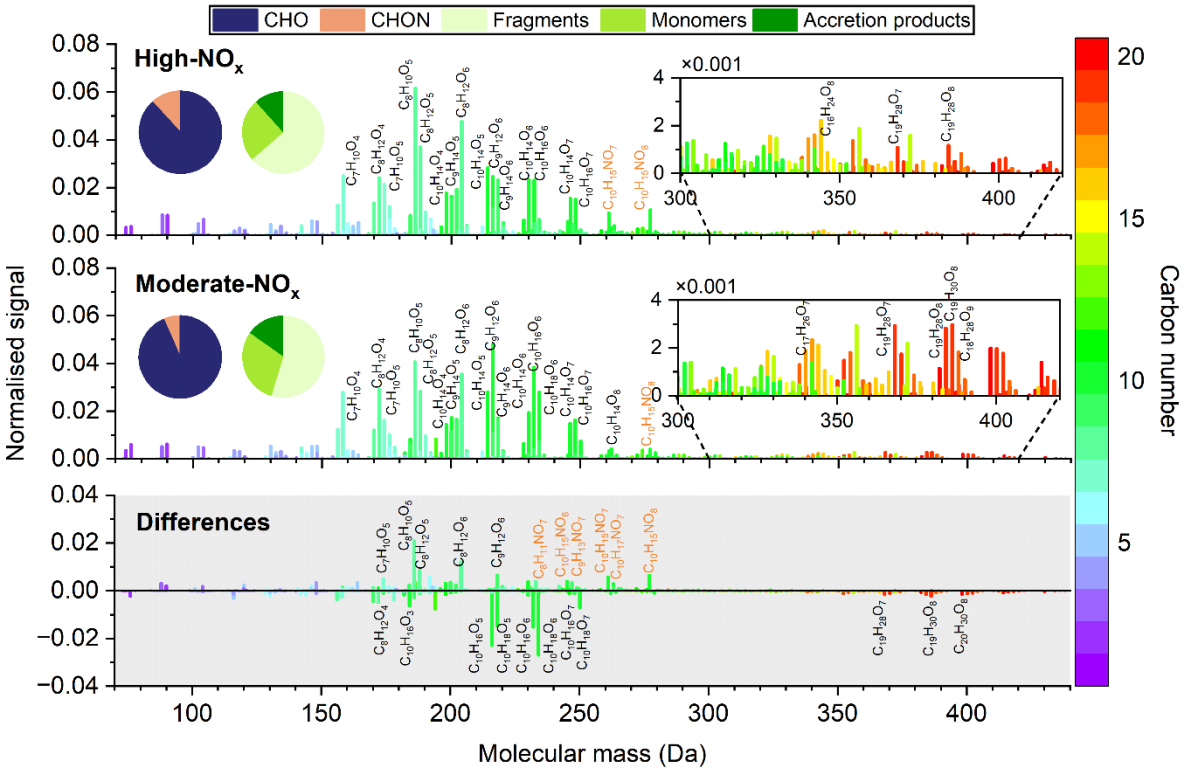

Figure 2: High-resolution mass spectra of particle-phase compounds measured by FIGAERO-CIMS in α-pinene experiments conducted under high- and moderate-NO_x conditions, and the corresponding difference spectra (high-NO_x minus moderate-NO_x). All signal intensities are normalised to 1. The pie charts on the left show the relative contributions of CHO and CHON compounds, while those on the right show the proportions of fragments (C < 10), monomers (C = 10), and accretion products (C > 10). The colour scale represents the number of carbon atoms in each compound.

https://doi.org/10.5194/egusphere-2026-2826
Preprint. Discussion started: 11 June 2026

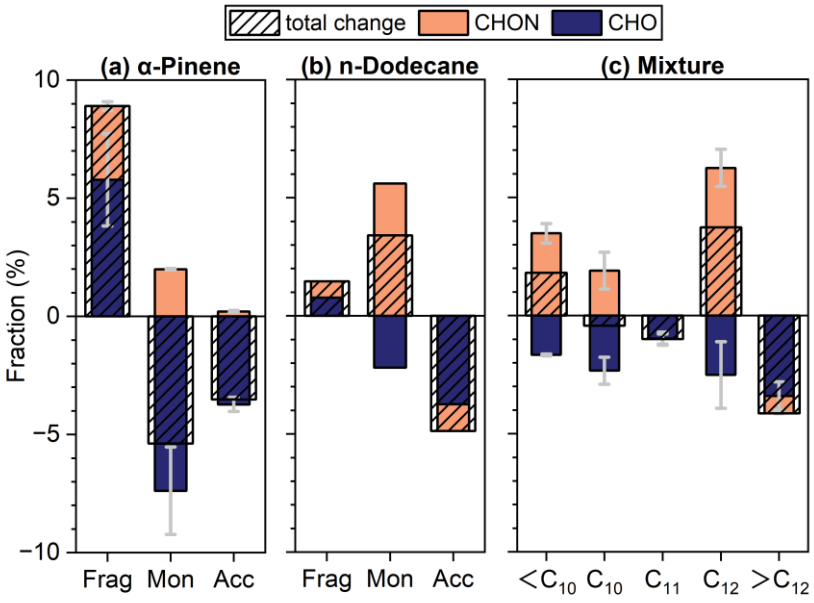

Figure 3: Fractional changes in particle-phase products grouped by carbon number under different NO_x conditions (high-NO_x minus moderate-NO_x) for (a) α-pinene, (b) n-dodecane, and (c) mixture systems. Hatched bars denote the total change, while solid bars represent the changes in the CHON and CHO fractions. Frag, Mon, and Acc refer to fragments, monomers, and accretion products, respectively. The error bars represent ±1 standard deviation derived from duplicate experiments.

https://doi.org/10.5194/egusphere-2026-2826
Preprint. Discussion started: 11 June 2026

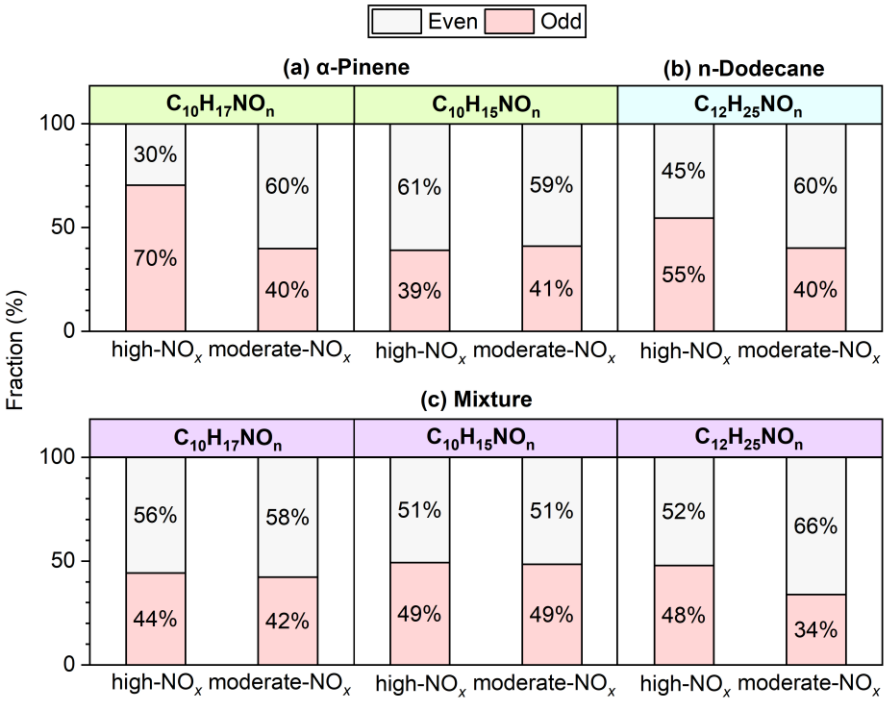

Figure 4: Fractions of even- and odd-oxygen $C_{10}H_{17}NO_n$, $C_{10}H_{15}NO_n$, and $C_{12}H_{25}NO_n$ compounds under moderate- and high-NO_x conditions in the (a) α-pinene, (b) n-dodecane, and (c) mixture systems.

https://doi.org/10.5194/egusphere-2026-2826
Preprint. Discussion started: 11 June 2026

3.2.2 n-Dodecane

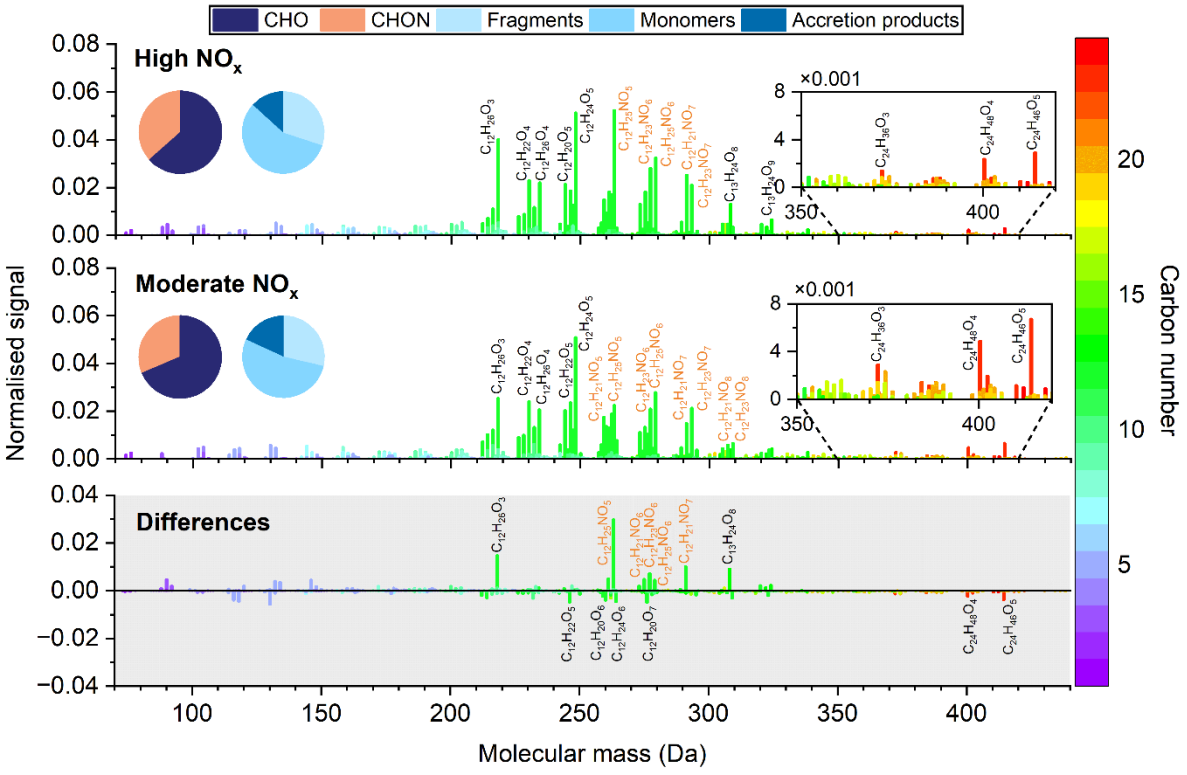

Figure 5: High-resolution mass spectra of particle-phase compounds measured by FIGAERO-CIMS in n-dodecane experiments conducted under high- and moderate-NO_x conditions, and the corresponding difference spectra (high-NO_x minus moderate-NO_x). All signal intensities are normalised to 1. The pie charts on the left show the relative contributions of CHO and CHON compounds, while those on the right show the proportions of fragments (C < 12), monomers (C = 12), and accretion products (C > 10). The colour scale represents the number of carbon atoms in each compound.

As shown in Fig. 5, particle-phase products derived from n-dodecane were primarily distributed in the molecular mass range of 210–310 Da.

Compared with the α-pinene system, the fraction of CHO compounds was lower in the n-dodecane system; however, CHO compounds still dominated the particle-phase composition under both conditions. CHON compounds accounted for 31 % of the total signal under moderate-NO_x conditions, increasing to 37 % under high-NO_x conditions.

https://doi.org/10.5194/egusphere-2026-2826
Preprint. Discussion started: 11 June 2026

n-Dodecane-derived products with fewer than 12 carbon atoms were classified as fragments, those with 12 carbon atoms as monomers, and those with more than 12 carbon atoms as accretion products. Under moderate-NO_x conditions, these groups contributed 29 %, 53 %, and 18 %, respectively, whereas under high-NO_x conditions, their fractions shifted to 30 %, 57 %, and 13 % (Fig. 5). Monomers were the dominant group, with the most abundant species including a series of CHO compounds such as $C_{12}H_{24}O_5$, $C_{12}H_{26}O_{3\text{-}4}$, and $C_{12}H_{22}O_{4\text{-}5}$, as well as CHON compounds such as $C_{12}H_{25}NO_{5\text{-}6}$ and $C_{12}H_{23}NO_{6\text{-}7}$. Among the accretion products, several C_{13} compounds (e.g. $C_{13}H_{24}O_{8\text{–}9}$) and C_{24} species (e.g., $C_{24}H_{46}O_5$) exhibited relatively strong signals.

As shown in Fig. 3b, NO_x also influenced the distribution of CHON and CHO compounds across carbon-number groups in the n-dodecane system; however, the resulting changes differed from those observed in the α-pinene system. Under high-NO_x conditions, changes in frag-CHO and frag-CHON fractions were small, both within ±1.0 percentage points. The proportion of mon-CHON increased by 5.6 percentage points, whereas mon-CHO decreased by 2.2 percentage points. The contribution of acc-CHO also declined by 3.7 percentage points.

Figure 4b shows the oxygen-number parity of $C_{12}H_{25}NO_n$ under moderate- and high-NO_x conditions. The fraction of $C_{12}H_{25}NO_n$ with an even number of oxygen atoms decreased from 60 % under moderate-NO_x conditions to 45 % under high-NO_x conditions.

3.2.3 Mixture

As shown in Fig. 6, the mixed-precursor system exhibited a broader molecular mass distribution than the single-precursor systems, with most compounds distributed within the range of 150–330 Da.

SOA particles formed in the mixture were dominated by CHO compounds, with the fraction of CHON species lying between those in the α-pinene and n-dodecane single-precursor systems. Under moderate-NO_x conditions, CHON compounds accounted for 19 % of the total signal, increasing to 31 % under high-NO_x conditions. This increase was substantially larger than that observed in the single-precursor systems.

Under moderate-NO_x conditions, fragments ($C < 10$), C_{10} compounds, C_{12} compounds, and accretion products ($C > 12$) contributed 39 %, 18 %, 24 %, and 16 % to the total signal, respectively, whereas under high-NO_x conditions, these proportions shifted to 40 %, 17 %, 28 %, and 12 % (Fig. 6). Fragments constituted the largest fraction under both conditions.

As shown in Fig. 3c, frag-CHO decreased by 1.7 percentage points, while frag-CHON increased by 3.5 percentage points, resulting in only a minor net change in the overall contribution of fragment product. Similarly, C_{10}-CHO decreased by 2.3 percentage points, whereas C_{10}-CHON increased by 1.9 percentage points, leaving the fraction of C_{10} compounds largely

https://doi.org/10.5194/egusphere-2026-2826
Preprint. Discussion started: 11 June 2026

unchanged. In contrast, the fraction of C_{12}-CHON compounds increased by 6.3 percentage points, representing the most pronounced change. The contribution of acc-CHO also decreased by 3.4 percentage points.

Figure 4c shows the oxygen-number parity of $C_{10}H_{17}NO_n$, $C_{10}H_{15}NO_n$, and $C_{12}H_{25}NO_n$ under moderate- and high- NO_x conditions. The fraction of $C_{10}H_{17}NO_n$ with an odd number of oxygen atoms increased slightly from 42 % under moderate-NO_x conditions to 44 % under high-NO_x conditions. The fraction of $C_{10}H_{15}NO_n$ with an even number of oxygen atoms remained largely unchanged. The fraction of $C_{12}H_{25}NO_n$ with an even number of oxygen atoms decreased from 66 % to 52 %.

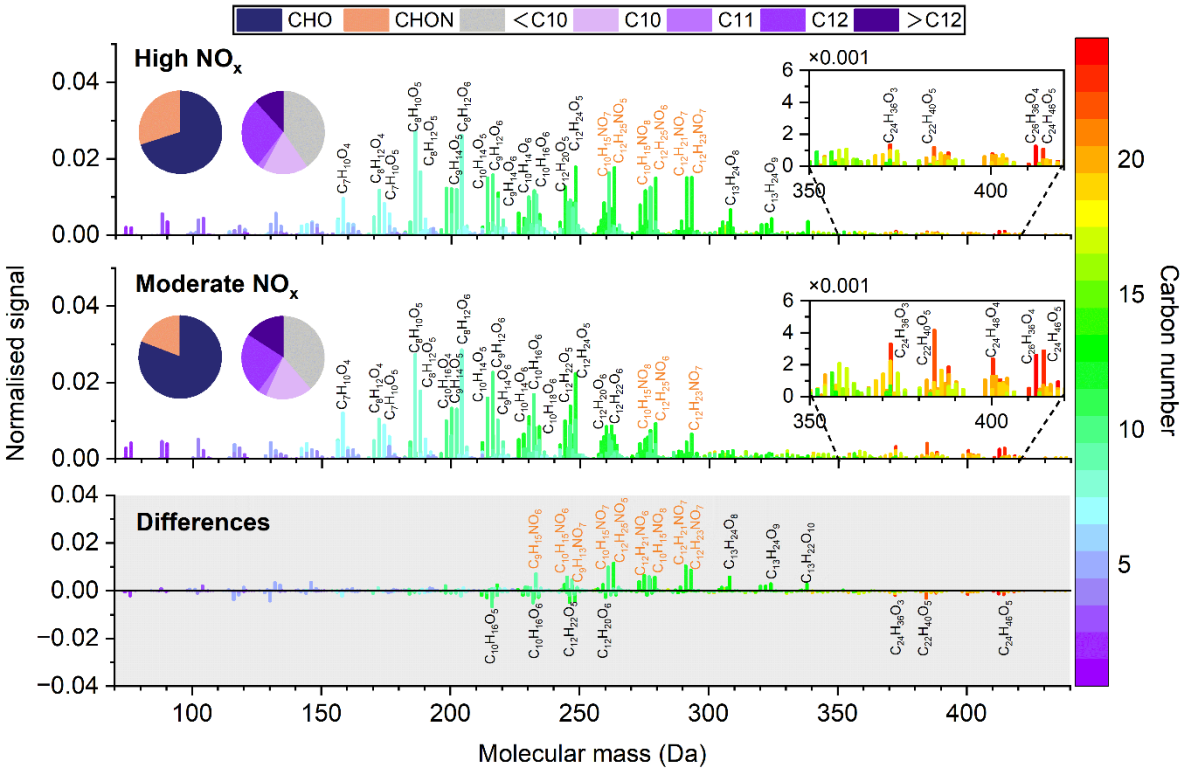

Figure 6: High-resolution mass spectra of particle-phase compounds measured by FIGAERO-CIMS in mixture experiments conducted under high- and moderate-NO_x conditions, and the corresponding difference spectra (high-NO_x minus moderate-NO_x). All signal intensities are normalised to 1. The pie charts on the left show the relative contributions of CHO and CHON compounds, while those on the right show the proportions of products with different carbon numbers. The colour scale represents the number of carbon atoms in each compound.

https://doi.org/10.5194/egusphere-2026-2826
Preprint. Discussion started: 11 June 2026

4 Discussion

4.1 NO_x effects on oxidant levels

Distinct differences in O_3 and OH concentrations were observed across the systems under different NO_x conditions (Figs. 1a and S2). Overall, O_3 concentrations were higher under high-NO_x conditions compared with moderate-NO_x conditions, consistent with enhanced RO_2 + NO reactions, which produce NO_2 and thereby facilitate O_3 formation. OH concentrations were also typically higher under high-NO_x conditions, reflecting the combined influence of multiple factors. Elevated O_3 levels provided an additional OH source via photolysis, while NO_x enhanced radical cycling and promoted OH regeneration. These effects more than compensated for OH loss through reaction with NO_2.

However, an exception was observed in the mixed-precursor system. During the first hour of the reaction, O_3 concentrations were comparable under both NO_x conditions, while OH concentrations were relatively low under high-NO_x conditions (Figs. 1a and S2). Consistently, higher concentrations of inorganic nitrates were observed under high-NO_x conditions (Fig. S4). This may indicate that OH loss through reaction with NO_2 played a more important role under high-NO_x conditions.

It should be noted that the inorganic nitrate concentrations were inferred from the nitrate signal measured by the AMS. For the C-ToF-AMS, nitrate quantification relies on the signals at m/z 30 and 46. However, the m/z 30 signal may include contributions from interfering fragments such as CH_2O^+ (Kiendler-Scharr et al., 2016). Furthermore, the use of the NO_2^+/NO^+ ratio (m/z 46/30) to estimate the inorganic and organic nitrate fractions may be influenced by other nitrogen-containing organic species, such as nitro compounds (Kiendler-Scharr et al., 2016). Therefore, the estimated inorganic nitrate concentrations may be subject to uncertainty. However, these results can still be used to compare differences between systems.

4.2 NO_x effects on the chemical composition of SOA particles in single-precursor systems

4.2.1 Formation of CHON compounds

CIMS results show that the fraction of CHON compounds was higher under high-NO_x conditions than under moderate-NO_x conditions in both the α-pinene and n-dodecane systems (Figs. 2 and 5). In addition, AMS-based estimates of organic nitrates within the measured total nitrate indicate that their concentrations were significantly enhanced under high-NO_x conditions (Fig. S5) (Kiendler-Scharr et al., 2016). These observations can be explained by shifts in RO_2 reaction pathways. NO competes with HO_2 and other RO_2 radicals for reactions with RO_2, thereby altering RO_2 branching. As NO_x concentrations increased, a larger fraction of RO_2 radicals reacted via RO_2 + NO pathway, increasing the likelihood of forming nitrogen-containing compounds.

https://doi.org/10.5194/egusphere-2026-2826
Preprint. Discussion started: 11 June 2026

In addition to the uncertainties associated with the estimation of organic nitrate concentrations from AMS measurements, CIMS also has inherent limitations in the detection of CHON compounds. In particular, its sensitivity towards CHON compounds with hydroxyl functional groups could be enhanced, potentially leading to an overestimation of their relative contribution (Iyer et al., 2016; Lee et al., 2014). Nevertheless, the two instruments exhibit consistent trends, providing confidence in the interpretation of the results.

Previous studies have reported that the mass fraction of organic nitrates in α-pinene-derived SOA can range from 6 % to 80 % of the total SOA mass (Berkemeier et al., 2020; Nozière et al., 1999; Rollins et al., 2010). Variations in oxidant conditions and α-pinene/NO_x ratios are important factors influencing organic nitrate yields. Zhao et al. (2018) reported that, at an initial α-pinene/NO_x ratio of around 1, organic nitrates accounted for approximately 11 % of the SOA particle mass. Pullinen et al. (2020) observed that organic nitrate mass fractions ranged from 0 % to 2.7 % under initial NO_x concentrations of 0.3–60 ppb, with the highest-NO_x condition corresponding to an α-pinene/NO_x ratio of 0.8. In the present study, decreasing the α-pinene/NO_x ratio from 2.2 to 1.0 increased the fraction of CHON compounds from 7 % to 12 %, consistent with the range reported in previous studies.

Studies directly reporting organic nitrate fractions formed from OH-initiated oxidation of n-dodecane are scarce. Fahnestock et al. (2015) observed that, under OH-initiated oxidation conditions, SOA mass increased by a factor of 2.3 as the system transitioned from low-NO (NO = 0) to high-NO (n-dodecane/NO = 2.5) conditions, accompanied by a substantial increase in nitrate formation. Consistent with these observations, in the present study, decreasing the n-dodecane/NO_x ratio from 2.7 to 0.8 led to an increase in the fraction of CHON compounds from 31 % to 37 %.

Compared with the α-pinene system, the n-dodecane system exhibited a higher fraction of CHON compounds. Previous studies have shown that organic nitrate yields generally increase with precursor molecular size (Yeh and Ziemann, 2014). In addition, electron-withdrawing functional groups, such as carbonyl and carboxyl groups located on or adjacent to the carbon atom bearing the peroxy radical group, tend to reduce organic nitrate yields, whereas electron-donating groups, such as hydroxyl groups, tend to enhance them (Ziemann and Atkinson, 2012). The Van-Krevelen distributions of SOA particles suggest that α-pinene-derived SOA contains a larger contribution from carbonyl- and carboxyl-containing compounds, whereas alcohol and peroxide functionalities likely play a more important role in the n-dodecane system (Fig. S6). These differences in chemical functionality may contribute to the higher CHON fraction observed in the n-dodecane system.

4.2.2 Role of alkoxy radical pathways in SOA formation

Formation of RO radicals represents an important branch of RO_2 + NO reactions. As described in Sect. 2.1, changes in fragment abundance and oxygen-number parity can be used as diagnostic indicators of the importance of RO reaction pathways.

https://doi.org/10.5194/egusphere-2026-2826
Preprint. Discussion started: 11 June 2026

For α-pinene, fragments accounted for more than 50 % of the total signal, indicating a substantial contribution from RO radical fragmentation (Fig. 2). Compared with moderate-NO_x conditions, the fractions of frag-CHO and frag-CHON compounds both increased significantly under high-NO_x conditions, suggesting an enhanced role of RO radical fragmentation pathways (Fig. 3). These fragments were dominated by C_8–C_9 compounds, including species such as $C_8H_{10,12}O_{5-6}$, $C_8H_{11}NO_7$, and $C_9H_{13}NO_7$. Similar trends have been reported in previous studies (Kang et al., 2025; Pullinen et al., 2020; Zhang et al., 2018).

In addition, in the α-pinene system, the fraction of $C_{10}H_{17}NO_n$ compounds with odd numbers of oxygen atoms increased markedly under high-NO_x conditions, while that of $C_{10}H_{15}NO_n$ compounds with even numbers of oxygen atoms increased slightly (Fig. 4). These changes may indicate a greater significance of the alkoxy-peroxy pathway. Together with the increased contribution of fragments, these observations suggest that RO radical chemistry played a more important role in SOA formation from α-pinene under high-NO_x conditions.

In the n-dodecane system, fragments accounted for a smaller fraction of the total signal than in the α-pinene system. The influence of NO_x on the relative abundance of fragments was much less pronounced, with increases in both frag-CHO and frag-CHON fractions remaining within 1 percentage point (Fig. 3). This suggests that, although RO_2 + NO reactions were enhanced under high-NO_x conditions, the resulting changes in RO fragmentation were not sufficient to substantially increase the contribution of fragment products.

In addition, the fraction of $C_{12}H_{25}NO_n$ compounds with even numbers of oxygen atoms decreased (Fig. 4). If additional alkoxy-peroxy steps occurred, a higher fraction of even-oxygen $C_{12}H_{25}NO_n$ would be expected. However, the observed trend showed the opposite behaviour. Under moderate-NO_x conditions, $C_{12}H_{25}NO_n$ compounds with even and odd numbers of oxygen atoms accounted for approximately 60 % and 40 % of the total $C_{12}H_{25}NO_n$ signal, respectively. This distribution suggests that a substantial fraction of RO_2 radicals may already have undergone one alkoxy-peroxy step prior to organic nitrate formation, leading to a dominance of even oxygen numbers. This is consistent with the strong propensity of n-dodecane-derived RO radicals to undergo isomerisation due to its long linear carbon chain. As NO_x concentrations increased, the probability of a second alkoxy-peroxy step may also have increased. Such an additional step would reverse the oxygen-number parity again, thereby increasing the relative contribution of odd-oxygen products.

Overall, higher NO_x concentrations shifted RO_2 reactions towards RO_2 + NO pathways, leading to an increased fraction of CHON compounds and a greater importance of RO radical chemistry. However, owing to intrinsic differences in precursor properties, the resulting changes in product distributions varied between systems. For α-pinene, first-generation RO radicals preferentially undergo fragmentation rather than isomerisation. Accordingly, increasing NO_x concentrations led to pronounced changes in the relative abundance of fragments. In contrast, RO radicals derived from n-dodecane are intrinsically more prone

https://doi.org/10.5194/egusphere-2026-2826
Preprint. Discussion started: 11 June 2026

to isomerisation. Under high-NO_x conditions, changes in fragment abundance remained small, while shifts in oxygen-number parity suggested the occurrence of additional alkoxy-peroxy steps.

4.3 NO_x effects on the chemical composition of SOA particles in mixed-precursor systems

In the mixed-precursor system, higher NO_x concentrations led to a substantial increase in the contribution of CHON compounds, with a larger enhancement than that observed in the single-precursor systems (Fig. 6). In particular, the fractions of frag-, C_{10}-, and C_{12}-CHON species all increased (Fig. 3). These results suggest a stronger contribution from RO_2 + NO termination pathways in the mixed-precursor system under high-NO_x conditions than in the single-precursor systems.

However, compared with the α-pinene single-precursor system, changes in fragment abundance and C_{10} oxygen-parity indicators were much weaker in the mixed-precursor system (Figs. 3 and 4). Under high-NO_x conditions, the increase in frag-CHON was partly offset by a decrease in frag-CHO, resulting in only a slight increase in the fraction of fragments (by ~1.8 percentage points) relative to moderate-NO_x conditions. At the same time, the fraction of odd-oxygen $C_{10}H_{17}NO_n$ increased slightly, while that of even-oxygen $C_{10}H_{15}NO_n$ remained largely unchanged.

Taken together, the increase in CHON fractions was not accompanied by a corresponding enhancement in α-pinene-derived RO radical pathway signatures. These observations suggest that, in the mixed-precursor system, higher NO_x concentrations more strongly favoured RO_2 + NO termination pathways, whereas their influence on α-pinene-derived RO chemistry remained comparatively limited.

4.4 Enhancement of SOA particle mass yields under elevated NO_x conditions

In this study, higher NO_x concentrations led to increased SOA particle mass yields across all systems. However, the magnitude of this increase was smaller in the mixed-precursor system than in the single-precursor systems.

NO_x exerts a dual role in SOA formation by altering both oxidant levels and the fate of RO_2 radicals, which together determine SOA particle mass yields (Pullinen et al., 2020; Pye et al., 2019). Under high-NO_x conditions, OH and O_3 concentrations were generally higher, which favoured SOA formation through enhanced oxidation (Figs. 1a and S2). At the same time, the fractions of CHON and fragments increased, while the contribution of accretion products decreased. Since products formed via RO_2 + NO reactions are generally more volatile than those formed via RO_2 + RO_2 and RO_2 + HO_2 pathways, this shift towards RO_2 + NO pathways would be expected to suppress SOA particle mass yields. In addition, enhanced alkoxy-peroxy pathway is expected to promote SOA formation.

https://doi.org/10.5194/egusphere-2026-2826
Preprint. Discussion started: 11 June 2026

Taken together, the positive effects of NO_x on oxidant levels and RO radical isomerisation appear to more than compensate for the negative impacts associated with enhanced formation of more volatile products via RO_2 + NO pathways, resulting in higher SOA particle mass yields under high-NO_x conditions across all systems. In the mixed-precursor system, however, the smaller enhancement in SOA particle mass yields under high-NO_x conditions may be related to the stronger enhancement in RO_2 + NO termination pathways together with the comparatively weaker contribution of α-pinene-derived alkoxy-peroxy pathway.

https://doi.org/10.5194/egusphere-2026-2826
Preprint. Discussion started: 11 June 2026

5 Conclusions and implications

This study investigated the effects of NO_x on SOA particle mass yields and chemical composition from α-pinene, n-dodecane, and their mixture under OH-dominated photooxidation conditions in the Manchester Aerosol Chamber. We evaluated how NO_x influences oxidant concentrations and radical reaction pathways, and how these effects differ between single- and mixed-precursor systems.

Across all systems, higher NO_x conditions resulted in elevated O_3 concentrations and generally higher OH levels, leading to enhanced precursor oxidation. In single-precursor systems, SOA particle mass yields approximately doubled under high-NO_x conditions. Molecular composition measurements further showed increased fractions of CHON compounds and fragmentation products, together with reduced contributions from accretion products under high-NO_x conditions, indicating a greater importance of RO_2 + NO reactions. At the same time, changes in the oxygen-number parity of representative product families suggest that RO isomerisation became more important. These observations indicate that enhanced oxidant production and RO isomerisation can more than compensate for the formation of more volatile products associated with RO_2 + NO termination pathways, resulting in a net enhancement of SOA formation.

In contrast, the response of the mixed-precursor system differed from those observed in the single-precursor systems. Although SOA particle mass yields also increased under high-NO_x conditions, the enhancement was less pronounced than would be expected from the responses of the individual precursor systems. Product distributions revealed a stronger increase in the fraction of CHON compounds, whereas this increase was not accompanied by corresponding enhancements in α-pinene-derived RO radical pathway signatures.

Previous laboratory studies have suggested that SOA particle mass yields from mixtures cannot always be predicted as a linear combination of the yields from their individual components (McFiggans et al., 2019; Voliotis et al., 2022). Our results provide further evidence for such non-linear behaviour under varying NO_x conditions and may help explain discrepancies between yields derived from linear additivity assumptions and those observed in real atmospheric environments. These findings emphasise the importance of accounting for the coexistence of multiple precursors in the presence of NO_x when developing SOA parameterisations for atmospheric models.

The present study focused on a single pair of representative biogenic and anthropogenic precursors under two NO_x regimes. Although the results show that the effects of NO_x in the mixture of α-pinene and n-dodecane cannot be directly inferred from behaviours observed in single-precursor systems, the extent to which these findings apply to other precursor combinations remains uncertain. Future studies incorporating a broader range of precursor mixtures and oxidant regimes will be needed to assess the generality of these results and their relevance to atmospheric SOA formation.

https://doi.org/10.5194/egusphere-2026-2826
Preprint. Discussion started: 11 June 2026

Data availability

All the data in the figures of this study are available upon request to the corresponding authors (g.mcfiggans@manchester.ac.uk and aristeidis.voliotis@manchester.ac.uk)

Author contribution

GX, AV, and GM conceived the study. GX and AV conducted the experiments. AV, TJB, YS, HW, DH provided assistance in instrument operation and data analysis. GX conducted the data analysis and wrote the manuscript with inputs from all the co-authors.

Competing interests

The contact author has declared that none of the authors has any competing interests.

Acknowledgements

Guangzhao Xie acknowledges the joint scholarship of The University of Manchester and China Scholarship Council (CSC) (grant no. 202208330060). Gordon McFiggans acknowledges funding from the Secondary Organic Aerosol Prediction in Realistic Atmospheres (SOAPRA) project (grant no. NE/V012665/1). Aristeidis Voliotis acknowledges funding support from the Natural Environment Research Council (NERC) through the UK National Centre for Atmospheric Science (NCAS). We acknowledge the use of ChatGPT (https://chatgpt.com/) for assistance in language refinement of this manuscript.

https://doi.org/10.5194/egusphere-2026-2826
Preprint. Discussion started: 11 June 2026

References

Andreae, M.O. and Crutzen, P.J.: Atmospheric aerosols: biogeochemical sources and role in atmospheric chemistry, Science, 276, 1052-1058, http://doi.org/10.1126/science.276.5315.1052, 1997.

Atkinson, R.: Atmospheric chemistry of VOCs and NOx, Atmos. Environ., 34, 2063-2101, http://doi.org/10.1016/s1352-2310(99)00460-4, 2000.

Atkinson, R.: Kinetics of the gas-phase reactions of OH radicals with alkanes and cycloalkanes, Atmos. Chem. Phys., 3, 2233-2307, http://doi.org/10.5194/acp-3-2233-2003, 2003.

Atkinson, R. and Arey, J.: Atmospheric Degradation of Volatile Organic Compounds, Chem. Rev., 103, 4605-4638, http://doi.org/10.1021/cr0206420, 2003.

Baltensperger, U., Kalberer, M., Dommen, J., Paulsen, D., Alfarra, M.R., Coe, H., Fisseha, R., Gascho, A., Gysel, M., Nyeki, S., Sax, M., Steinbacher, M., Prevot, A.S.H., Sjogren, S., Weingartner, E. and Zenobi, R.: Secondary organic aerosols from anthropogenic and biogenic precursors, Faraday Discuss., 130, 265-278, http://doi.org/10.1039/b417367h, 2005.

Bannan, T.J., Le Breton, M., Priestley, M., Worrall, S.D., Bacak, A., Marsden, N.A., Mehra, A., Hammes, J., Hallquist, M., Alfarra, M.R., Krieger, U.K., Reid, J.P., Jayne, J., Robinson, W., McFiggans, G., Coe, H., Percival, C.J. and Topping, D.: A method for extracting calibrated volatility information from the FIGAERO-HR-ToF-CIMS and its experimental application, Atmos. Meas. Tech., 12, 1429-1439, http://doi.org/10.5194/amt-12-1429-2019, 2019.

Berkemeier, T., Takeuchi, M., Eris, G. and Ng, N.L.: Kinetic modeling of formation and evaporation of secondary organic aerosol from NO3 oxidation of pure and mixed monoterpenes, Atmos. Chem. Phys., 20, 15513-15535, http://doi.org/10.5194/acp-20-15513-2020, 2020.

Berndt, T., Richters, S., Jokinen, T., Hyttinen, N., Kurtén, T., Otkjær, R.V., Kjaergaard, H.G., Stratmann, F., Herrmann, H., Sipilä, M., Kulmala, M. and Ehn, M.: Hydroxyl radical-induced formation of highly oxidized organic compounds, Nat. Commun., 7, 13677, http://doi.org/10.1038/ncomms13677, 2016.

Bianchi, F., Kurten, T., Riva, M., Mohr, C., Rissanen, M.P., Roldin, P., Berndt, T., Crounse, J.D., Wennberg, P.O., Mentel, T.F., Wildt, J., Junninen, H., Jokinen, T., Kulmala, M., Worsnop, D.R., Thornton, J.A., Donahue, N., Kjaergaard, H.G. and Ehn, M.: Highly Oxygenated Organic Molecules (HOM) from Gas-Phase Autoxidation Involving Peroxy Radicals: A Key Contributor to Atmospheric Aerosol, Chem. Rev., 119, 3472-3509, http://doi.org/10.1021/acs.chemrev.8b00395, 2019.

Chen, T.Z., Zhang, P., Ma, Q.X., Chu, B.W., Liu, J., Ge, Y.L. and He, H.: Smog Chamber Study on the Role of NOx in SOA and O3 Formation from Aromatic Hydrocarbons, Environ. Sci. Technol., http://doi.org/10.1021/acs.est.2c04022, 2022.

Clapp, L.J. and Jenkin, M.E.: Analysis of the relationship between ambient levels Of O3, NO2 and NO as a function of NOχ in the UK, Atmos. Environ., 35, 6391-6405, http://doi.org/10.1016/s1352-2310(01)00378-8, 2001.

Dash, M.R., Balaganesh, M. and Rajakumar, B.: Rate coefficients for the gas-phase reaction of OH radical with α-pinene: an experimental and computational study, Mol. Phys., 112, 1495-1511, http://doi.org/10.1080/00268976.2013.840395, 2014.

Dibble, T.S.: Reactions of the Alkoxy Radicals Formed Following OH-Addition to α-Pinene and β-Pinene. C−C Bond Scission Reactions, Journal of the American Chemical Society, 123, 4228-4234, http://doi.org/10.1021/ja003553i, 2001.

Drewnick, F., Hings, S.S., Alfarra, M.R., Prevot, A.S.H. and Borrmann, S.: Aerosol quantification with the Aerodyne Aerosol Mass Spectrometer: detection limits and ionizer background effects, Atmos. Meas. Tech., 2, 33-46, http://doi.org/10.5194/amt-2-33-2009, 2009.

Eddingsaas, N.C., Loza, C.L., Yee, L.D., Chan, M., Schilling, K.A., Chhabra, P.S., Seinfeld, J.H. and Wennberg, P.O.: alpha-pinene photooxidation under controlled chemical conditions - Part 2: SOA yield and composition in low- and high-NOx environments, Atmos. Chem. Phys., 12, 7413-7427, http://doi.org/10.5194/acp-12-7413-2012, 2012.

Ehn, M., Thornton, J.A., Kleist, E., Sipila, M., Junninen, H., Pullinen, I., Springer, M., Rubach, F., Tillmann, R., Lee, B., Lopez-Hilfiker, F., Andres, S., Acir, I.H., Rissanen, M., Jokinen, T., Schobesberger, S., Kangasluoma, J., Kontkanen, J., Nieminen, T., Kurten, T., Nielsen, L.B., Jorgensen, S., Kjaergaard, H.G., Canagaratna, M., Dal Maso, M., Berndt, T., Petaja, T., Wahner, A., Kerminen, V.M., Kulmala, M., Worsnop, D.R., Wildt, J. and Mentel, T.F.: A large source of low-volatility secondary organic aerosol, Nature, 506, 476-+, http://doi.org/10.1038/nature13032, 2014.

https://doi.org/10.5194/egusphere-2026-2826
Preprint. Discussion started: 11 June 2026

Fahnestock, K.A.S., Yee, L.D., Loza, C.L., Coggon, M.M., Schwantes, R., Zhang, X., Dalleska, N.F. and Seinfeld, J.H.: Secondary Organic Aerosol Composition from C-12 Alkanes, J. Phys. Chem. A, 119, 4281-4297, http://doi.org/10.1021/jp501779w, 2015.

Hallquist, M., Wenger, J.C., Baltensperger, U., Rudich, Y., Simpson, D., Claeys, M., Dommen, J., Donahue, N.M., George, C., Goldstein, A.H., Hamilton, J.F., Herrmann, H., Hoffmann, T., Iinuma, Y., Jang, M., Jenkin, M.E., Jimenez, J.L., Kiendler-Scharr, A., Maenhaut, W., McFiggans, G., Mentel, T.F., Monod, A., Prevot, A.S.H., Seinfeld, J.H., Surratt, J.D., Szmigielski, R. and Wildt, J.: The formation, properties and impact of secondary organic aerosol: current and emerging issues, Atmos. Chem. Phys., 9, 5155-5236, http://doi.org/10.5194/acp-9-5155-2009, 2009.

Iyer, S., Lopez-Hilfiker, F., Lee, B.H., Thornton, J.A. and Kurtén, T.: Modeling the Detection of Organic and Inorganic Compounds Using Iodide-Based Chemical Ionization, The Journal of Physical Chemistry A, 120, 576-587, http://doi.org/10.1021/acs.jpca.5b09837, 2016.

Jenkin, M.E., Saunders, S.M. and Pilling, M.J.: The tropospheric degradation of volatile organic compounds: a protocol for mechanism development, Atmos. Environ., 31, 81-104, http://doi.org/10.1016/S1352-2310(96)00105-7, 1997.

Jimenez, J.L., Canagaratna, M.R., Donahue, N.M., Prevot, A.S.H., Zhang, Q., Kroll, J.H., DeCarlo, P.F., Allan, J.D., Coe, H., Ng, N.L., Aiken, A.C., Docherty, K.S., Ulbrich, I.M., Grieshop, A.P., Robinson, A.L., Duplissy, J., Smith, J.D., Wilson, K.R., Lanz, V.A., Hueglin, C., Sun, Y.L., Tian, J., Laaksonen, A., Raatikainen, T., Rautiainen, J., Vaattovaara, P., Ehn, M., Kulmala, M., Tomlinson, J.M., Collins, D.R., Cubison, M.J., Dunlea, E.J., Huffman, J.A., Onasch, T.B., Alfarra, M.R., Williams, P.I., Bower, K., Kondo, Y., Schneider, J., Drewnick, F., Borrmann, S., Weimer, S., Demerjian, K., Salcedo, D., Cottrell, L., Griffin, R., Takami, A., Miyoshi, T., Hatakeyama, S., Shimono, A., Sun, J.Y., Zhang, Y.M., Dzepina, K., Kimmel, J.R., Sueper, D., Jayne, J.T., Herndon, S.C., Trimborn, A.M., Williams, L.R., Wood, E.C., Middlebrook, A.M., Kolb, C.E., Baltensperger, U. and Worsnop, D.R.: Evolution of Organic Aerosols in the Atmosphere, Science, 326, 1525-1529, http://doi.org/10.1126/science.1180353, 2009.

Johnson, D. and Marston, G.: The gas-phase ozonolysis of unsaturated volatile organic compounds in the troposphere, Chem. Soc. Rev., 37, 699-716, http://doi.org/10.1039/B704260B, 2008.

Kanakidou, M., Seinfeld, J.H., Pandis, S.N., Barnes, I., Dentener, F.J., Facchini, M.C., Van Dingenen, R., Ervens, B., Nenes, A., Nielsen, C.J., Swietlicki, E., Putaud, J.P., Balkanski, Y., Fuzzi, S., Horth, J., Moortgat, G.K., Winterhalter, R., Myhre, C.E.L., Tsigaridis, K., Vignati, E., Stephanou, E.G. and Wilson, J.: Organic aerosol and global climate modelling: a review, Atmos. Chem. Phys., 5, 1053-1123, http://doi.org/10.5194/acp-5-1053-2005, 2005.

Kang, S., Wildt, J., Pullinen, I., Vereecken, L., Wu, C., Wahner, A., Zorn, S.R. and Mentel, T.F.: Formation of highly oxygenated organic molecules from α-pinene photooxidation: evidence for the importance of highly oxygenated alkoxy radicals, Atmos. Chem. Phys., 25, 15715-15740, http://doi.org/10.5194/acp-25-15715-2025, 2025.

Kelly, J.M., Doherty, R.M., O'Connor, F.M. and Mann, G.W.: The impact of biogenic, anthropogenic, and biomass burning volatile organic compound emissions on regional and seasonal variations in secondary organic aerosol, Atmos. Chem. Phys., 18, 7393-7422, http://doi.org/10.5194/acp-18-7393-2018, 2018.

Kiendler-Scharr, A., Mensah, A.A., Friese, E., Topping, D., Nemitz, E., Prevot, A.S.H., Äijälä, M., Allan, J., Canonaco, F., Canagaratna, M., Carbone, S., Crippa, M., Dall Osto, M., Day, D.A., De Carlo, P., Di Marco, C.F., Elbern, H., Eriksson, A., Freney, E., Hao, L., Herrmann, H., Hildebrandt, L., Hillamo, R., Jimenez, J.L., Laaksonen, A., McFiggans, G., Mohr, C., O'Dowd, C., Otjes, R., Ovadnevaite, J., Pandis, S.N., Poulain, L., Schlag, P., Sellegri, K., Swietlicki, E., Tiitta, P., Vermeulen, A., Wahner, A., Worsnop, D. and Wu, H.-C.: Ubiquity of organic nitrates from nighttime chemistry in the European submicron aerosol, Geophys. Res. Lett., 43, 7735-7744, http://doi.org/10.1002/2016GL069239, 2016.

Krechmer, J., Lopez-Hilfiker, F., Koss, A., Hutterli, M., Stoermer, C., Deming, B., Kimmel, J., Warneke, C., Holzinger, R., Jayne, J., Worsnop, D., Fuhrer, K., Gonin, M. and de Gouw, J.: Evaluation of a New Reagent-Ion Source and Focusing Ion-Molecule Reactor for Use in Proton-Transfer-Reaction Mass Spectrometry, Anal. Chem., 90, 12011-12018, http://doi.org/10.1021/acs.analchem.8b02641, 2018.

Kroll, J.H. and Seinfeld, J.H.: Chemistry of secondary organic aerosol: Formation and evolution of low-volatility organics in the atmosphere, Atmos. Environ., 42, 3593-3624, http://doi.org/10.1016/j.atmosenv.2008.01.003, 2008.

Lane, T.E., Donahue, N.M. and Pandis, S.N.: Effect of NOx on Secondary Organic Aerosol Concentrations, Environ. Sci. Technol., 42, 6022-6027, http://doi.org/10.1021/es703225a, 2008.

https://doi.org/10.5194/egusphere-2026-2826
Preprint. Discussion started: 11 June 2026

Lee, A., Goldstein, A.H., Kroll, J.H., Ng, N.L., Varutbangkul, V., Flagan, R.C. and Seinfeld, J.H.: Gas-phase products and secondary aerosol yields from the photooxidation of 16 different terpenes, J. Geophys. Res. Atmos., 111, http://doi.org/10.1029/2006jd007050, 2006.

Lee, B.H., Lopez-Hilfiker, F.D., Mohr, C., Kurtén, T., Worsnop, D.R. and Thornton, J.A.: An Iodide-Adduct High-Resolution Time-of-Flight Chemical-Ionization Mass Spectrometer: Application to Atmospheric Inorganic and Organic Compounds, Environ. Sci. Technol., 48, 6309-6317, http://doi.org/10.1021/es500362a, 2014.

Lim, Y.B. and Ziemann, P.J.: Effects of Molecular Structure on Aerosol Yields from OH Radical-Initiated Reactions of Linear, Branched, and Cyclic Alkanes in the Presence of NOx, Environ. Sci. Technol., 43, 2328-2334, http://doi.org/10.1021/es803389s, 2009.

Lopez-Hilfiker, F.D., Mohr, C., Ehn, M., Rubach, F., Kleist, E., Wildt, J., Mentel, T.F., Lutz, A., Hallquist, M., Worsnop, D. and Thornton, J.A.: A novel method for online analysis of gas and particle composition: description and evaluation of a Filter Inlet for Gases and AEROsols (FIGAERO), Atmos. Meas. Tech., 7, 983-1001, http://doi.org/10.5194/amt-7-983-2014, 2014.

Loza, C.L., Craven, J.S., Yee, L.D., Coggon, M.M., Schwantes, R.H., Shiraiwa, M., Zhang, X., Schilling, K.A., Ng, N.L., Canagaratna, M.R., Ziemann, P.J., Flagan, R.C. and Seinfeld, J.H.: Secondary organic aerosol yields of 12-carbon alkanes, Atmos. Chem. Phys., 14, 1423-1439, http://doi.org/10.5194/acp-14-1423-2014, 2014.

McFiggans, G., Mentel, T.F., Wildt, J., Pullinen, I., Kang, S., Kleist, E., Schmitt, S., Springer, M., Tillmann, R., Wu, C., Zhao, D.F., Hallquist, M., Faxon, C., Le Breton, M., Hallquist, A.M., Simpson, D., Bergstrom, R., Jenkin, M.E., Ehn, M., Thornton, J.A., Alfarra, M.R., Bannan, T.J., Percival, C.J., Priestley, M., Topping, D. and Kiendler-Scharr, A.: Secondary organic aerosol reduced by mixture of atmospheric vapours, Nature, 565, 587-593, http://doi.org/10.1038/s41586-018-0871-y, 2019.

Ng, N.L., Chhabra, P.S., Chan, A.W.H., Surratt, J.D., Kroll, J.H., Kwan, A.J., McCabe, D.C., Wennberg, P.O., Sorooshian, A., Murphy, S.M., Dalleska, N.F., Flagan, R.C. and Seinfeld, J.H.: Effect of NOx level on secondary organic aerosol (SOA) formation from the photooxidation of terpenes, Atmos. Chem. Phys., 7, 5159-5174, http://doi.org/10.5194/acp-7-5159-2007, 2007.

Nie, W., Yan, C., Yang, L., Roldin, P., Liu, Y., Vogel, A.L., Molteni, U., Stolzenburg, D., Finkenzeller, H., Amorim, A., Bianchi, F., Curtius, J., Dada, L., Draper, D.C., Duplissy, J., Hansel, A., He, X.-C., Hofbauer, V., Jokinen, T., Kim, C., Lehtipalo, K., Nichman, L., Mauldin, R.L., Makhmutov, V., Mentler, B., Mizelli-Ojdanic, A., Petäjä, T., Quéléver, L.L.J., Schallhart, S., Simon, M., Tauber, C., Tomé, A., Volkamer, R., Wagner, A.C., Wagner, R., Wang, M., Ye, P., Li, H., Huang, W., Qi, X., Lou, S., Liu, T., Chi, X., Dommen, J., Baltensperger, U., El Haddad, I., Kirkby, J., Worsnop, D., Kulmala, M., Donahue, N.M., Ehn, M. and Ding, A.: NO at low concentration can enhance the formation of highly oxygenated biogenic molecules in the atmosphere, Nat. Commun., 14, 3347, http://doi.org/10.1038/s41467-023-39066-4, 2023.

Nozière, B., Barnes, I. and Becker, K.-H.: Product study and mechanisms of the reactions of α-pinene and of pinonaldehyde with OH radicals, 104, 23645-23656, http://doi.org/https://doi.org/10.1029/1999JD900778, 1999.

Orlando, J.J., Tyndall, G.S. and Wallington, T.J.: The Atmospheric Chemistry of Alkoxy Radicals, Chem. Rev., 103, 4657-4690, http://doi.org/10.1021/cr020527p, 2003.

Pathak, R.K., Stanier, C.O., Donahue, N.M. and Pandis, S.N.: Ozonolysis of alpha-pinene at atmospherically relevant concentrations: Temperature dependence of aerosol mass fractions (yields), J. Geophys. Res. Atmos., 112, http://doi.org/10.1029/2006jd007436, 2007.

Pospisilova, V., Lopez-Hilfiker, F.D., Bell, D.M., El Haddad, I., Mohr, C., Huang, W., Heikkinen, L., Xiao, M., Dommen, J., Prevot, A.S.H., Baltensperger, U. and Slowik, J.G.: On the fate of oxygenated organic molecules in atmospheric aerosol particles, Sci. Adv., 6, eaax8922, http://doi.org/doi:10.1126/sciadv.aax8922, 2020.

Pullinen, I., Schmitt, S., Kang, S., Sarrafzadeh, M., Schlag, P., Andres, S., Kleist, E., Mentel, T.F., Rohrer, F., Springer, M., Tillmann, R., Wildt, J., Wu, C., Zhao, D., Wahner, A. and Kiendler-Scharr, A.: Impact of NOx on secondary organic aerosol (SOA) formation from α-pinene and β-pinene photooxidation: the role of highly oxygenated organic nitrates, Atmos. Chem. Phys., 20, 10125-10147, http://doi.org/10.5194/acp-20-10125-2020, 2020.

Pusede, S.E., Steiner, A.L. and Cohen, R.C.: Temperature and Recent Trends in the Chemistry of Continental Surface Ozone, Chem. Rev., 115, 3898-3918, http://doi.org/10.1021/cr5006815, 2015.

https://doi.org/10.5194/egusphere-2026-2826
Preprint. Discussion started: 11 June 2026

Pye, H.O.T., D'Ambro, E.L., Lee, B.H., Schobesberger, S., Takeuchi, M., Zhao, Y., Lopez-Hilfiker, F., Liu, J., Shilling, J.E., Xing, J., Mathur, R., Middlebrook, A.M., Liao, J., Welti, A., Graus, M., Warneke, C., de Gouw, J.A., Holloway, J.S., Ryerson, T.B., Pollack, I.B. and Thornton, J.A.: Anthropogenic enhancements to production of highly oxygenated molecules from autoxidation, Proc. Natl. Acad. Sci. U.S.A., 116, 6641-6646, http://doi.org/doi:10.1073/pnas.1810774116, 2019.

Ramanathan, V., Crutzen, P.J., Kiehl, J.T. and Rosenfeld, D.: Atmosphere - Aerosols, climate, and the hydrological cycle, Science, 294, 2119-2124, http://doi.org/10.1126/science.1064034, 2001.

Robinson, A.L., Donahue, N.M., Shrivastava, M.K., Weitkamp, E.A., Sage, A.M., Grieshop, A.P., Lane, T.E., Pierce, J.R. and Pandis, S.N.: Rethinking organic aerosols: Semivolatile emissions and photochemical aging, Science, 315, 1259-1262, http://doi.org/10.1126/science.1133061, 2007.

Rollins, A.W., Smith, J.D., Wilson, K.R. and Cohen, R.C.: Real Time In Situ Detection of Organic Nitrates in Atmospheric Aerosols, Environ. Sci. Technol., 44, 5540-5545, http://doi.org/10.1021/es100926x, 2010.

Sarrafzadeh, M., Wildt, J., Pullinen, I., Springer, M., Kleist, E., Tillmann, R., Schmitt, S.H., Wu, C., Mentel, T.F., Zhao, D., Hastie, D.R. and Kiendler-Scharr, A.: Impact of NOx and OH on secondary organic aerosol formation from β-pinene photooxidation, Atmos. Chem. Phys., 16, 11237-11248, http://doi.org/10.5194/acp-16-11237-2016, 2016.

Shao, Y.Q., Wang, Y., Du, M., Voliotis, A., Alfarra, M.R., O'Meara, S.P., Turner, S.F. and McFiggans, G.: Characterisation of the Manchester Aerosol Chamber facility, Atmos. Meas. Tech., 15, 539-559, http://doi.org/10.5194/amt-15-539-2022, 2022.

Srivastava, D., Vu, T.V., Tong, S., Shi, Z. and Harrison, R.M.: Formation of secondary organic aerosols from anthropogenic precursors in laboratory studies, npj Clim. Atmos. Sci., 5, 22, http://doi.org/10.1038/s41612-022-00238-6, 2022.

Stirnweis, L., Marcolli, C., Dommen, J., Barmet, P., Frege, C., Platt, S.M., Bruns, E.A., Krapf, M., Slowik, J.G., Wolf, R., Prévôt, A.S.H., Baltensperger, U. and El-Haddad, I.: Assessing the influence of NOx concentrations and relative humidity on secondary organic aerosol yields from α-pinene photo-oxidation through smog chamber experiments and modelling calculations, Atmos. Chem. Phys., 17, 5035-5061, http://doi.org/10.5194/acp-17-5035-2017, 2017.

Vereecken, L. and Peeters, J.: Nontraditional (Per)oxy Ring-Closure Paths in the Atmospheric Oxidation of Isoprene and Monoterpenes, The Journal of Physical Chemistry A, 108, 5197-5204, http://doi.org/10.1021/jp049219g, 2004.

Vereecken, L. and Peeters, J.: A structure–activity relationship for the rate coefficient of H-migration in substituted alkoxy radicals, Physical Chemistry Chemical Physics, 12, 12608-12620, http://doi.org/10.1039/C0CP00387E, 2010.

Voliotis, A., Du, M., Wang, Y., Shao, Y.Q., Alfarra, M.R., Bannan, T.J., Hu, D.W., Pereira, K.L., Hamilton, J.F., Hallquist, M., Mentel, T.F. and McFiggans, G.: Chamber investigation of the formation and transformation of secondary organic aerosol in mixtures of biogenic and anthropogenic volatile organic compounds, Atmos. Chem. Phys., 22, 14147-14175, http://doi.org/10.5194/acp-22-14147-2022, 2022.

Voliotis, A., Wang, Y., Shao, Y.Q., Du, M., Bannan, T.J., Percival, C.J., Pandis, S.N., Alfarra, M.R. and McFiggans, G.: Exploring the composition and volatility of secondary organic aerosols in mixed anthropogenic and biogenic precursor systems, Atmos. Chem. Phys., 21, 14251-14273, http://doi.org/10.5194/acp-21-14251-2021, 2021.

Wang, N.X., Jorga, S.D., Pierce, J.R., Donahue, N.M. and Pandis, S.N.: Particle wall-loss correction methods in smog chamber experiments, Atmos. Meas. Tech., 11, 6577-6588, http://doi.org/10.5194/amt-11-6577-2018, 2018.

Wang, Z., Ehn, M., Rissanen, M.P., Garmash, O., Quéléver, L., Xing, L., Monge-Palacios, M., Rantala, P., Donahue, N.M., Berndt, T. and Sarathy, S.M.: Efficient alkane oxidation under combustion engine and atmospheric conditions, Communications Chemistry, 4, 18, http://doi.org/10.1038/s42004-020-00445-3, 2021.

Xie, G., Voliotis, A., Bannan, T.J., Shao, Y., Wu, H., Hu, D. and McFiggans, G.: The impact of CO on secondary organic aerosols formed from the mixture of α-pinene and n-dodecane, EGUsphere, 2025, 1-27, http://doi.org/10.5194/egusphere-2025-4841, 2025.

Yeh, G.K. and Ziemann, P.J.: Alkyl Nitrate Formation from the Reactions of C8–C14 n-Alkanes with OH Radicals in the Presence of NOx: Measured Yields with Essential Corrections for Gas–Wall Partitioning, The Journal of Physical Chemistry A, 118, 8147-8157, http://doi.org/10.1021/jp500631v, 2014.

Yuan, B., Koss, A.R., Warneke, C., Coggon, M., Sekimoto, K. and de Gouw, J.A.: Proton-Transfer-Reaction Mass Spectrometry: Applications in Atmospheric Sciences, Chem. Rev., 117, 13187-13229, http://doi.org/10.1021/acs.chemrev.7b00325, 2017.

https://doi.org/10.5194/egusphere-2026-2826
Preprint. Discussion started: 11 June 2026

766 Zhang, H., Yee, L.D., Lee, B.H., Curtis, M.P., Worton, D.R., Isaacman-VanWertz, G., Offenberg, J.H., Lewandowski, M.,
767 Kleindienst, T.E., Beaver, M.R., Holder, A.L., Lonneman, W.A., Docherty, K.S., Jaoui, M., Pye, H.O.T., Hu, W., Day,
768 D.A., Campuzano-Jost, P., Jimenez, J.L., Guo, H., Weber, R.J., de Gouw, J., Koss, A.R., Edgerton, E.S., Brune, W.,
769 Mohr, C., Lopez-Hilfiker, F.D., Lutz, A., Kreisberg, N.M., Spielman, S.R., Hering, S.V., Wilson, K.R., Thornton, J.A.
770 and Goldstein, A.H.: Monoterpenes are the largest source of summertime organic aerosol in the southeastern United
771 States, 115, 2038-2043, http://doi.org/doi:10.1073/pnas.1717513115, 2018.
772 Zhang, X., Schwantes, R.H., Coggon, M.M., Loza, C.L., Schilling, K.A., Flagan, R.C. and Seinfeld, J.H.: Role of ozone in
773 SOA formation from alkane photooxidation, Atmos. Chem. Phys., 14, 1733-1753, http://doi.org/10.5194/acp-14-
774 1733-2014, 2014.
775 Zhao, D.F., Schmitt, S.H., Wang, M.J., Acir, I.H., Tillmann, R., Tan, Z.F., Novelli, A., Fuchs, H., Pullinen, I., Wegener, R.,
776 Rohrer, F., Wildt, J., Kiendler-Scharr, A., Wahner, A. and Mentel, T.F.: Effects of NOx and SO2 on the secondary
777 organic aerosol formation from photooxidation of α-pinene and limonene, Atmos. Chem. Phys., 18, 1611-1628,
778 http://doi.org/10.5194/acp-18-1611-2018, 2018.
779 Ziemann, P.J. and Atkinson, R.: Kinetics, products, and mechanisms of secondary organic aerosol formation, Chem. Soc. Rev.,
780 41, 6582-6605, http://doi.org/10.1039/c2cs35122f, 2012.
781